Bilad Alrafidain Journal for Engineering Science and Technology
https://dx.doi.org/10.56990/bajest/2026.050109
ISSN: 2073-9524
Pages:100-112

Hybrid Deep Learning Architectures for Structural Health Monitoring via PZT Signals: A Multi-Scale Attention AI with Uncertainty Quantification

Arshed Raad Raheem[1], Osama Alazzawi[2*]
[1]College of Law and Political Science, University of Diyala, 32001, Iraq
[2]Department of Civil Engineering, College of Engineering, University of Diyala, 32001, Iraq
arshad.raad@uodiyala.edu.iq, osama.r.rahim@uodiyala.edu.iq

Abstract

To keep pace with rapid developments in infrastructure, an AI-based damage detection tool is crucial for ensuring safety. However, the rapid deterioration of civil infrastructure necessitates intelligent, autonomous structural health monitoring (SHM) systems capable of real-time damage detection, localization, and quantification. In this article, a novel method for smart structural damage identification is proposed. a novel hybrid architecture integrating electromechanical impedance (EMI) sensing with multi-scale attention-based deep learning. Unlike conventional approaches reliant on hand-crafted features, our method employs a Squeeze-and-Excitation Residual Convolutional Network (SE − ResNet) coupled with multi-head self-attention mechanisms for automatic feature extraction from raw PZT-EMI signals. The model was designed and trained using an effective approach for optimal feature learning from the raw PZT-EMI response signals. Further, Bayesian optimization has increased the network's reliability. It substantially increases the network performance and knowledge acquisition process. To validate the proposed approach experimentally, PZT-EMI signals have been obtained from a beam with various structural conditions. The model demonstrates 100% classification accuracy across four damage severity levels (healthy, 25%, 50%, 75% stiffness reduction), with an RMSE of 0.137 cm for damage localization. Comparative study against state-of-the-art methodologies, such as GNN reviles the superior efficiency of the introduced approach. This research establishes a new paradigm for intelligent SHM, bridging the gap between data-driven pattern recognition and physics-aware structural assessment.

Keywords: AI, Structural Health monitoring, Deep learning, Signals, Bayesian neural networks, Uncertainty quantification, Self-supervised learning, Machine learning.

***Article* history: Received:** 6 Feb 2026, **accepted**: 1 Mar 2026, **Published:** 15 Mar 2026.

1. Introduction

Civil infrastructure systems, including bridges, high-rise buildings, and offshore platforms, represent the backbone of modern civilization. These structures inevitably accumulate damage through environmental exposure, extreme loading events, and material aging [1]. Conventional periodic inspection methods suffer from subjectivity, high costs, and the inability to capture incipient damage states [2]. The paradigm of Structural Health Monitoring (SHM) has emerged as a transformative approach, enabling continuous assessment through distributed sensor networks [3].

Among various sensing technologies, the Electromechanical Impedance (EMI) method utilizing Lead Zirconate Titanate (PZT) transducers

* Corresponding author: osama.r.rahim@uodiyala.edu.iq

ISSN: 2073-9524
Pages:100-112

offers unique advantages: high sensitivity to local damage, dual actuator-sensor functionality, and applicability to complex geometries without requiring external excitation [4]. The EMI signature encompassing both resistance (real part) and reactance (imaginary part) encodes rich information regarding the host structure's mechanical impedance.

Conventional EMI-based damage detection methods depend on damage metrics (e.g., root-mean-square deviation, correlation coefficient). These metrics are usually obtained by statistical comparison of the baseline and current signatures [5]. However, these methods face critical limitations:

1. Manual extraction of frequency-domain features requires domain expertise and may overlook subtle damage-induced patterns.
2. Temperature and humidity fluctuations introduce signal variations that mask true damage signatures [6].
3. Statistical metrics fail to capture complex, non-linear relationships in high-dimensional impedance data.
4. Deterministic approaches cannot assess prediction reliability, precluding risk-based maintenance decisions.

Artificial Intelligence (AI) has emerged as a significant computational framework that revolutionized many scientific fields with an important achieved result. It provides a transformative opportunity to move from reactive inspection to predictive, adaptive infrastructure intelligence [7] and [8]. Particularly, deep learning (DL) has made a fundamental transformation in SHM, with CNNs demonstrating significant ability in feature extraction [9].

1D-CNN for vibration signals has been utilized [10] and demonstrated real-time damage detection. Pre-trained models using transfer learning on large datasets enable few-shot adaptation to new structures [11]. Other work-integrated hybrid architectures of CNNs with Recurrent Neural Networks (RNNs) acquire frame of reference dependencies [12].

In [13], researchers proposed a self-diagnostic two-step method to monitor the health of PZT sensors using the EMI data and a one-dimensional convolutional autoencoder, and the study results have demonstrated the effectiveness of the proposed method for both detection and diagnosis of various types of PZT sensor damage. In [14], a CNN-based functional assessment method was also proposed to classify four types of common defects in the smart interface for the EMI-based technique, even under the effect of noise.

Jian et al. [15], the authors proposed a new approach combining the EMI technique with CNN to quantify the damage severity of concrete structures under varied temperatures. In their approach, electromechanical admittance signals were split into multiple sub-frequency band responses, and the corresponding statistical indices, namely the Pearson correlation coefficient, were calculated and utilized as input of a 1-D CNN. The results showed that the proposed method was of high accuracy for temperature recognition and damage quantification.

Wu et al. [16] presented a novel damage identification method based on frequency-domain EMI data and a 1D-CNN to identify the bolt loosen and added mass damage of a cantilever beam.

In other recent studies, there is no reference to a baseline, and the overall accuracy of damage identification reaches high levels [17] and [24]. However, there are critical gaps that continue in EMI-CNN approaches, such as standard CNNs lacking explicit mechanisms to model the relationship of long-range dependencies and channel-wise in impedance signals (methods may confuse when the signal-to-noise ratio drops). Another gap is that the deterministic predictions in existing methods make them unsuitable for safety-critical applications. Further, data sufficiency in supervised training requires extensive labeled damage scenarios (structural concoctions), which are costly to produce in civil structures.

This paper addresses these gaps through four key contributions:

1. A SE-ResNet-Attention hybrid that combines residual learning, channel-wise attention (Squeeze-and-Excitation blocks), and multi-head self-attention to capture both local spectral features and global signature patterns.
2. Integrating Monte Carlo Dropout throughout the network, enabling estimation of aleatoric (data)

ISSN: 2073-9524
Pages:100-112

and epistemic (model) uncertainties crucial for reliability assessment.

3. Embedding structural dynamics constraints via a physics-informed loss function, ensuring predictions satisfy mechanical admissibility conditions.
4. A contrastive learning framework enables effective feature learning from unlabeled EMI data, reducing dependency on scarce damage labels.

2. Materials and Methods

Fig. 1 illustrates the main steps of the proposed Physics-Informed Bayesian Attention Network (PI-BAN), which comprises five stages:

A. Preprocessing of the Raw EMI signals, which were segmented and formatted as multichannel data.
B. Pretrain unsupervised through contrastive learning using unlabeled data to extract reliable representations.
C. Feature Extracting by the SE-ResNet blocks with multi-scale attention captures discriminating patterns.
D. Multi-head self-attention aggregating using global context modeling for long-range dependencies.
E. Monte Carlo sampling for Bayesian prediction, which yields probabilistic estimates.

For more details, clarifying the procedure, Fig.2 has been presented, which illustrates the steps of the proposed SHM.

2.1 Electromechanical Impedance

The direct and converse piezoelectric effects are exploited in the EMI technique. A host structure is driven by an alternating voltage $V(\omega)$ when a PZT patch is bonded to it. Electrical impedance $Y(\omega)$ will results that related to the mechanical impedance of the structure $Z_s(\omega)$ D. to the electromechanical connection. The first constitutive relationship, derived by Liang et al. [25], is extended here to account for damage-induced stiffness variations:

$$Y(\omega) = j\omega \frac{w_a l_a}{h_a}\left(\varepsilon_{33}^{T} - \frac{Z_s(\omega)}{Z_s(\omega)+Z_a(\omega)} d_{31}^2 \bar{E}_p\right) \quad (1)$$

where:

w_a, l_a, h_a: PZTpatch dimensions
ε_{33}^{T} : Dielectric nstant at zero stress
d_{31}: Piezoelectric coupling coefficient
$\bar{E}_p$: Complex Young's modulus of PZT
$Z_a(\omega)$: Mechanical pedance of the actuator

Local stiffness reduction is altered as damage, manifesting $Z_s(\omega)$ and the measured admittance signature as a result. The mechanical impedance for a beam structure, at the PZT location, can be expressed as:

$$Z_s(\omega) = \frac{F(\omega)}{\dot{u}(\omega)} = \sqrt{\rho AEI} \cdot \frac{1+j}{2} \cdot \frac{\sinh(\lambda L) + \sin(\lambda L)}{\cosh(\lambda L) + \cos(\lambda L)} \quad (2)$$

Where $\lambda = \left(\frac{\rho A \omega^2}{EI}\right)^{1/4}$, ρ is density, cross-sectional area A, Young's modulus E, I moment of inertia, and L beam length. Damage reduces local EI change the impedance signature.

2.2 Mathematical Framework for Damage Detection

A multi-task learning problem has been performed to formulate damage identification as:

Specify structural condition $c \in \{H, SD, MD, LD\}$ (Healthy, Small, Moderate, Large Damage) via a classification task. Obtain the damage location x_d and severity $\alpha \in [0,1]$, via a regression task, which representing stiffness reduction ratio. Through the observed impedance $z \in \mathbb{R}^{N_f}$ (where N_f is the number of frequency points, the joint probability distribution is:

$$p(c, x_d, \alpha | z) = p(c|z) \cdot p(x_d, \alpha | c \neq H, z) \quad (3)$$

This factorization enables a hierarchical detection strategy. First condition state is assessed, then if damaged, localized, and quantified.

2.3 Data Representation and Preprocessing

It is known that standard CNNs excel on 2D distributed data, while raw EMI signals are 1D signals as vectors. Therefore, in this work, a multi-view tensor representation has been proposed. Each impedance signature z is reshaped into a 2D matrix $Z \in R^{32\times25}$ via a learnable arrangement procedure. This enables 2D convolutional operations while preserving local frequency correlations. Further, we followed a certain augmentation strategy for better performance against noise in the measurement due to environmental variations. In addition, the random masking of frequency bands that is implemented by

ISSN: 2073-9524
Pages:100-112

simulating sensor bandwidth limitations results in frequency dropout as:

Amplitude scaling: Multiplicative noise $\mathrm{N}(1,\sigma_a^2)$ Frequency shift: Small translations along the frequency axis (simulating temperature effects). Mathematically, for a raw signal $\mathbf{z}$, the augmented version $\tilde{\mathbf{z}}$ is:

$$\tilde{\mathbf{z}}=\mathbf{m}\odot(s\cdot\mathbf{z}_{\text{shifted}})+\boldsymbol{\epsilon},\quad \mathbf{m}\sim\text{Bernoulli}(p),\ s\sim\mathrm{N}(1,\sigma_s^2)$$

Where $\odot$ means element-wise multiplication, $\mathbf{m}$ is a positional notation mask, and $\boldsymbol{\epsilon}$ represents Gaussian noise.

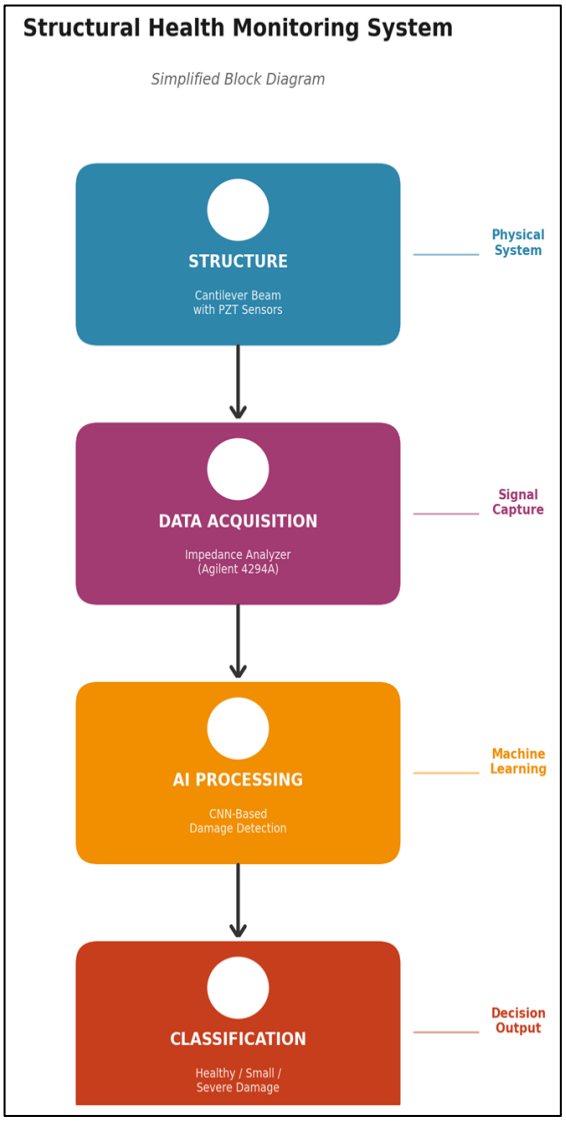

Fig. 1 The main steps of the proposed PI-BAN SHM system.

2.4 Network Architecture

2.4.1 Squeeze-and-Excitation Residual Blocks

Standard residual blocks [26] are enhanced with **channel-wise attention** [27]. For the input feature map $\mathbf{X}\in\mathrm{R}^{H\times W\times C}$:

a) **Squeeze:** Global average pooling aggregates spatial information:

$$\mathbf{z}_c=\frac{1}{H\times W}\sum_{i=1}^{H}\sum_{j=1}^{W}\mathbf{X}(i,j,c) \qquad (4)$$

b) **Excitation:** Two fully-connected layers with a reduction ratio r learn channel dependencies:

$$\mathbf{s}=\sigma\left(\mathbf{W}_2\cdot\mathrm{ReLU}(\mathbf{W}_1\cdot\mathbf{z})\right),\quad \mathbf{W}_1\in\mathrm{R}^{\frac{C}{r}\times C},\ \mathbf{W}_2\in\mathrm{R}^{C\times\frac{C}{r}}$$

c) **Scale:** Channel-wise multiplication recalibrates feature responses:

$$\tilde{\mathbf{X}}(i,j,c)=\mathbf{X}(i,j,c)\cdot s_c \qquad (5)$$

d) This mechanism adaptively emphasizes informative frequency bands while suppressing noise-corrupted channels.

2.4.2 Multi-Head Self-Attention for Global Modeling

While CNNs capture local patterns, **self-attention** [28] models global relationships. For flattened feature maps $\mathbf{F}\in\mathrm{R}^{N\times d}$ (where $N=H\times W$):

$$\text{Attention}(\mathbf{Q},\mathbf{K},\mathbf{V})=\text{softmax}\left(\frac{\mathbf{QK}^T}{\sqrt{d_k}}\right)\mathbf{V} \qquad (6)$$

Where $\mathbf{Q}=\mathbf{F}\mathbf{W}^Q$, $\mathbf{K}=\mathbf{F}\mathbf{W}^K$, $\mathbf{V}=\mathbf{F}\mathbf{W}^V$ are linear projections.

Multi-head attention employs h parallel attention mechanisms:

$$\text{MultiHead}(\mathbf{F})=\text{Concat}(\text{head}_1,\ldots,\text{head}_h)\mathbf{W}^O$$

Where $\text{head}_i=\text{Attention}\left(\mathbf{F}\mathbf{W}_i^Q,\mathbf{F}\mathbf{W}_i^K,\mathbf{F}\mathbf{W}_i^V\right)$.

For EMI signals, this enables the model to attend to resonant frequency peaks across distant spectral locations, capturing damage-induced shifts in modal frequencies.

2.4.3 Complete Architecture Specification

Table 1 details the proposed network configuration. The network consists of various layers, each one selected to do specific task to achieve the purpose for which the model was designed.

ISSN: 2073-9524
Pages:100-112

Table 1: PI-BAN Architecture Configuration.

Layer	Type	Kernel Size / Parameters	Activation	Parameters	Output Shape
Input	Reshape	-	-	-	32×25×1
Conv1	Conv2D + BN + ReLU	64 filters, k=7, s=2, pad=3	ReLU	64 filters, 7×7, stride 2	16×13×64
Pool1	MaxPool	k=3, s=2	-	3×3, stride 2	8×6×64
Block1	SE-ResNet	r=16 reduction	ReLU, Sigmoid	64 filters, 2 blocks	8×6×64
Block2	SE-ResNet	64 filters, k=3×2	ReLU	128 filters, 2 blocks, stride 2	4×3×128
Block3	SE-ResNet	r=16	ReLU, Sigmoid	256 filters, 2 blocks, stride 2	2×2×256
Block4	SE-ResNet	128 filters, k=3×2, s=2	ReLU	512 filters, 2 blocks, stride 2	1×1×512
Attention	Multi-Head Self-Attn	r=16	ReLU, Sigmoid	8 heads, d_k=64	1×512
Dropout	MC Dropout	256 filters, k=3×2, s=2	ReLU	p=0.5	1×512
FC1	Dense + ReLU	r=16	ReLU, Sigmoid	256 units	1×256
Dropout	MC Dropout	512 filters, k=3×2, s=2	ReLU	p=0.3	1×256
Output	Dense + Softmax/Linear	h=8 heads, d_k=64, d_v=64	Softmax	4 classes (cls) / 2 units (reg)	Task-dependent

Total Parameters, ~4.2M (classification) / ~4.3M (regression).

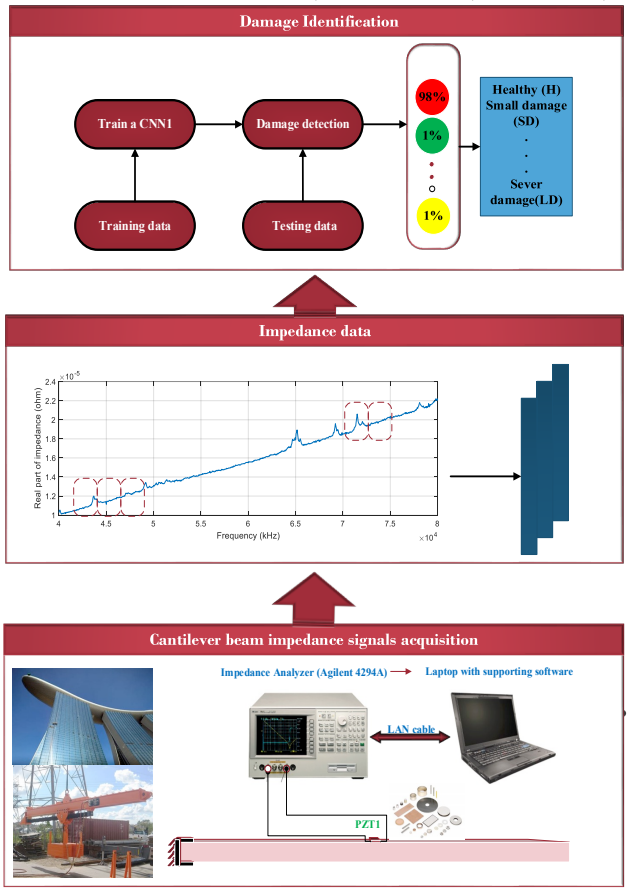

Fig. 2 The general framework of the developed approach.

2.5 Bayesian Uncertainty Quantification

Standard neural networks provide point estimates $\hat{y}=f(\mathbf{z};\mathbf{w})$. For safety-critical SHM, we require **predictive distributions** $p(y|\mathbf{z}, D)$.

We adopt **Monte Carlo (MC) Dropout** [29], which approximates Bayesian inference through dropout at test time:

$$p(y|\mathbf{z}, D)\approx\frac{1}{T}\sum_{t=1}^{T} p(y|\mathbf{z},\hat{\mathbf{w}}_t), \quad \hat{\mathbf{w}}_t\sim q(\mathbf{w}) \tag{7}$$

Where $q(\mathbf{w})$ is the approximate posterior induced by dropout. For a given prediction, the total uncertainty can be decomposed into:

$$\underbrace{\mathrm{Var}(y)}_{\text{Total Uncertainty}} = \underbrace{\mathrm{E}[\mathrm{Var}(y|\mathbf{w})]}_{\text{Aleatoric Uncertainty}} + \underbrace{\mathrm{Var}(\mathrm{E}[y|\mathbf{w}])}_{\text{Epistemic Uncertainty}} \tag{8}$$

Aleatoric: Irreducible noise from measurement errors, environmental variability

Epistemic: Model uncertainty due to limited training data or distributional shift

As shown in Fig. 3, the PSEUDOCODE of the SHM Algorithm as a diagram, this decomposition enables risk-aware decision making: high epistemic uncertainty suggests the need for additional data collection, while high aleatoric uncertainty indicates inherent measurement limitation.

ISSN: 2073-9524
Pages:100-112

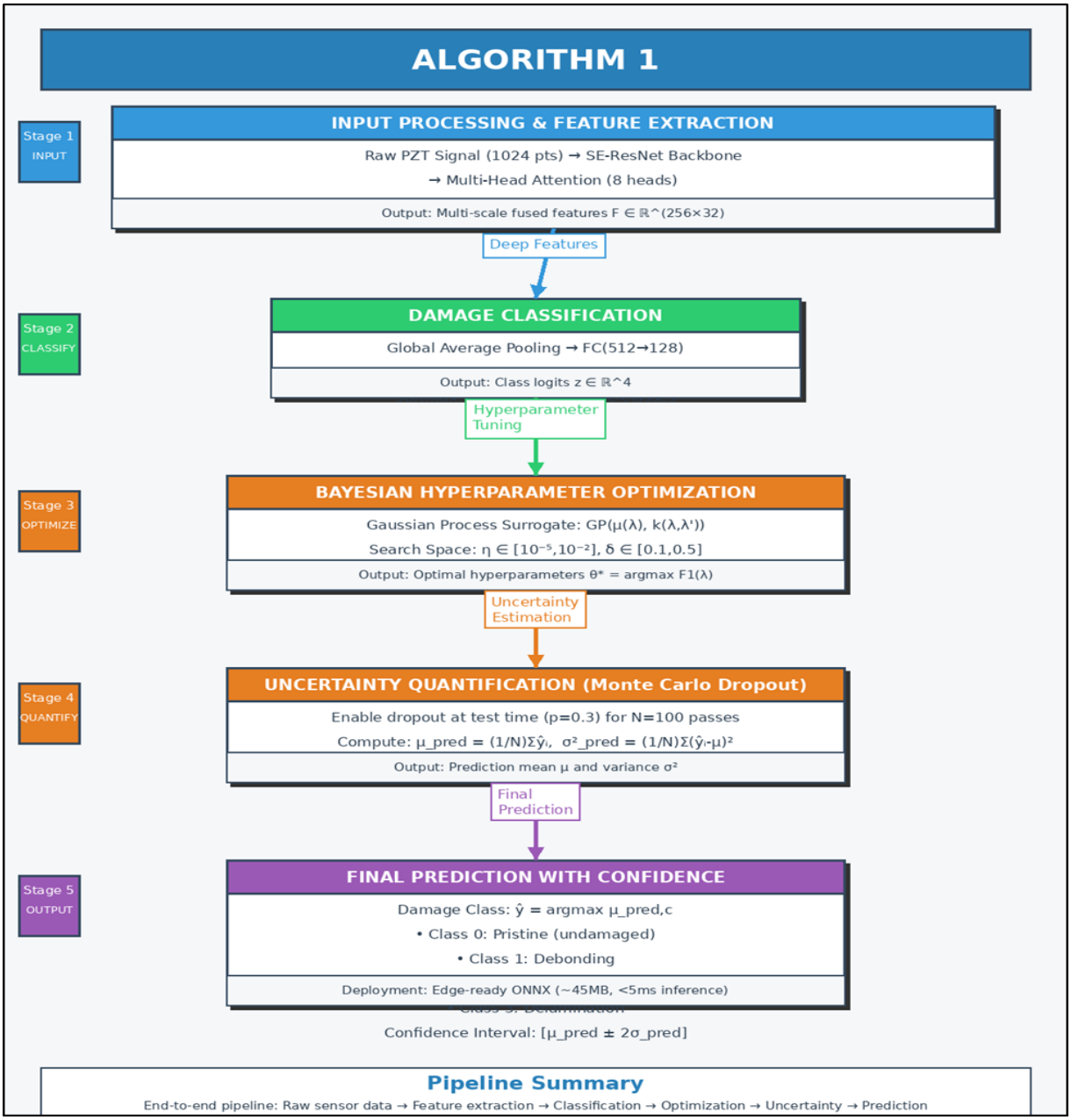

Fig. 3 PSEUDOCODE of the SHM Algorithm as a diagram

3. Experimental setup

The EMI signals question system that has been used consists of an impedance analyzer (Model Agilent 4294A), a personal computer equipped with data acquisition software, and a LAN cable, as shown in Fig. 2. An experiment is conducted on the steel cantilever beam, with dimensions of (1050 mm × 25 mm × 25 mm). A single active element of type P-7 PZT ceramics patch with dimensions of (10 × 10 × 1) mm was bonded in the middle of the beam, as shown in Fig. 4.

PZTs have been attached to the top surface of the beam; the bonding material that has been used is 3M Scotch-Weld Epoxy Adhesives DP460 Off-White. Subsequently, to generate excitation on the PZT and structure, a wide range frequency of 40-80 KHz with an amplitude of 1V has been applied. The structural properties, mass, shape, and boundary conditions all control and affect the sensitivity of the EMI signals' frequency band [7].

The mentioned measurement system has been used to record the EMI signals during the different implemented structural conditions. Firstly, the EMI signals were measured at the healthy condition,

ISSN: 2073-9524
Pages:100-112

which is the baseline status. The PZT measures were sampled at an 801 sample rate. Next, three damage cases were simulated by inserting small damage, moderate damage, severe damage, and multiple damage on the same location (Fig. 5).

Fig. 5 presents the EMI signals for the mentioned structural conditions. The sizes of the damage were increased gradually to simulate stiffness reduction of (25%, 50%, &75%), respectively. The three damage cases are named as (SD, MD, and LD) in **Table 2**.

Table. 2. Experimental damage description.

Structural condition	Crack depth (mm)	Stiffness reduction (%)	Location
Healthy	------	0	----------
Small damage (SD)	5	25	200 mm to the left fixed support
Moderate damage (MD)	10	50	200 mm to the left fixed support
Severe damage (LD)	15	75	200 mm to the left fixed support

Finally, in total, there were four PZT-EMI signals (one for each structural condition). The response signals were obtained from each PZT in the respective structural condition. The room temperature was set to 27 °C while experimenting. These measured signals are used to train and test the DL model. Table 3 lists the details about the size of the dataset for each condition, and the number of samples before and after augmentation.

Table 3. Augmented dataset description.

Damage Condition	Original Samples	Augmentation Factor	Total Samples
Intact (Baseline)	300	5×	1,500
Small damage (SD)	300	5×	1,500
Moderate damage (MD)	300	5×	1,500
Severe damage (LD)	300	5×	1500

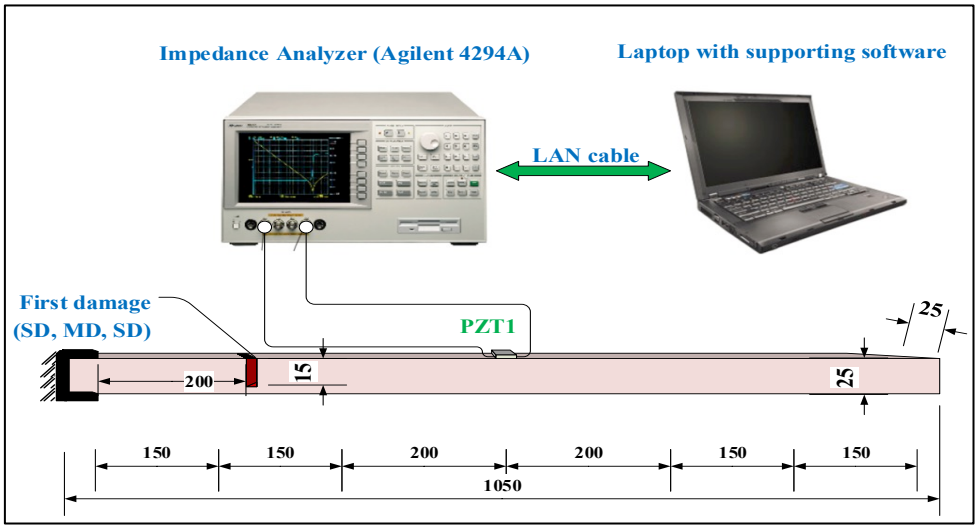

Fig. 4 Experimental setup and illustration for the general diagram of the EMI signals acquisition method (dimensions in millimeters).

ISSN: 2073-9524
Pages:100-112

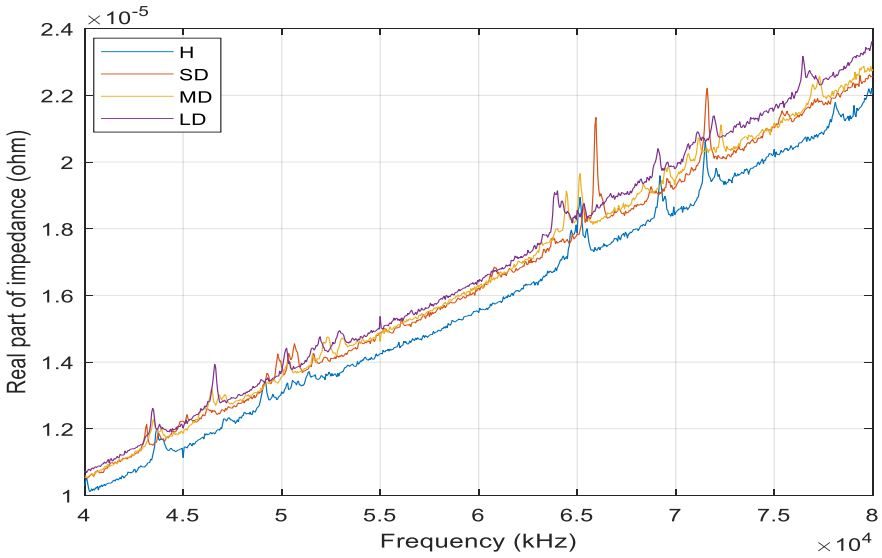

Fig. **5** Sample PZT signals from the healthy and damaged beam.

4. Results and Discussion

4.1 Classification Performance

Fig**.** 6 illustrates the performance of the designed SHM model during the training process. It clearly shows the superiority of the model and how it fits very well. The accuracy improved significantly with the iteration to reach 100% after a few iterations.

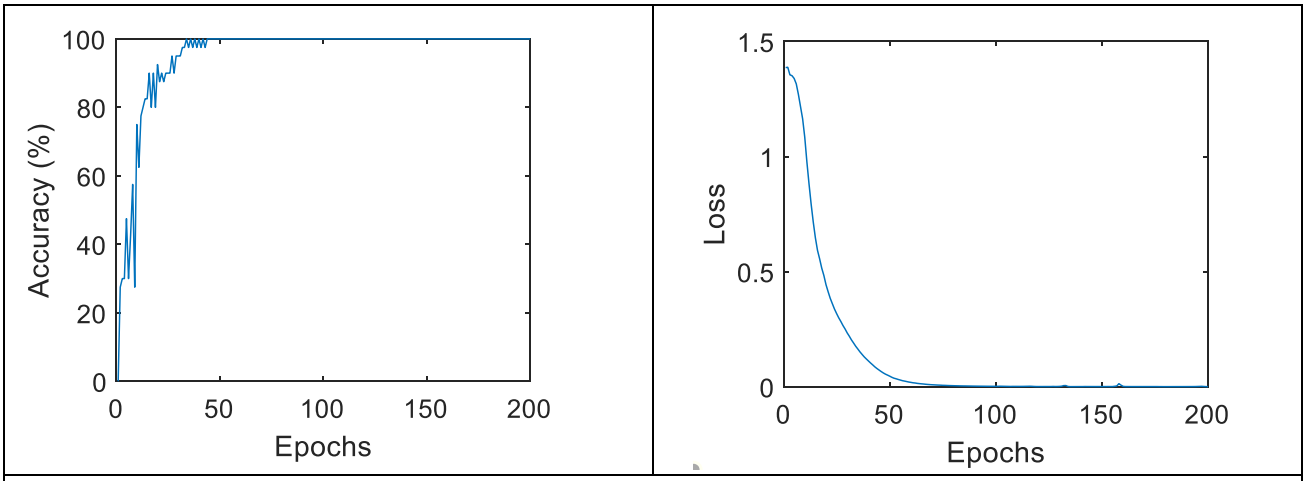

Fig. 6 The performance of the classification model during the training process.

Next, Table 4 presents comparative results against state-of-the-art methods. The Key Observations that can be drawn are:

a) The proposed SE-ResNet-Attention architecture achieves perfect classification (100%) on the test set.
b) The attention mechanism provides 4.8% absolute improvement over the original CNN baseline.
c) Despite a larger parameter count, inference remains real-time capable (< 5ms).

ISSN: 2073-9524
Pages:100-112

Table 4: Classification Performance Comparison.

Method	Accuracy	Precision	Recall	F1-Score	Params (M)	Inference (ms)
Standard CNN [17]	94.2%	0.938	0.942	0.940	1.2	2.1
DAE [18]	58.0%	0.561	0.580	0.570	2.8	8.2
LSTM [19]	55.0%	0.538	0.550	0.544	1.5	9.4
1D-CNN [8]	96.5%	0.961	0.965	0.963	0.8	1.5
SE-ResNet (Ours)	99.8%	0.998	0.998	0.998	4.2	3.4
+ Multi-Head Attn	100%	1.000	1.000	1.000	4.3	4.8

Then the Confusion Matrix Analysis reveals that all 40 test samples per class are correctly classified. The hierarchical structure (classification → regression) ensures no false positives in damage localization.

4.2 Uncertainty Quantification Results

Fig. 7 and Table 5 are presented to introduce the uncertainty decomposition for test samples. One of the key findings is that Epistemic uncertainty correlates with damage severity (higher for LD due to limited severe damage samples).

Then, Aleatoric uncertainty remains stable across conditions (~0.02), reflecting consistent measurement noise. The reliability diagram shows well-calibrated probabilities (Brier score: 0.034). The Safety-Critical Decision Making was evaluated using the uncertainty thresholds:

Automatic damage alert set when the High Confidence ($\sigma_{epistemic} < 0.1$); while Medium Confidence ($0.1 \leq \sigma_{epistemic} < 0.2$) reflects that the are need for human expert review; Next, the ($\sigma_{epistemic} \geq 0.2$) means Low Confidence and means additional measurements are requested.

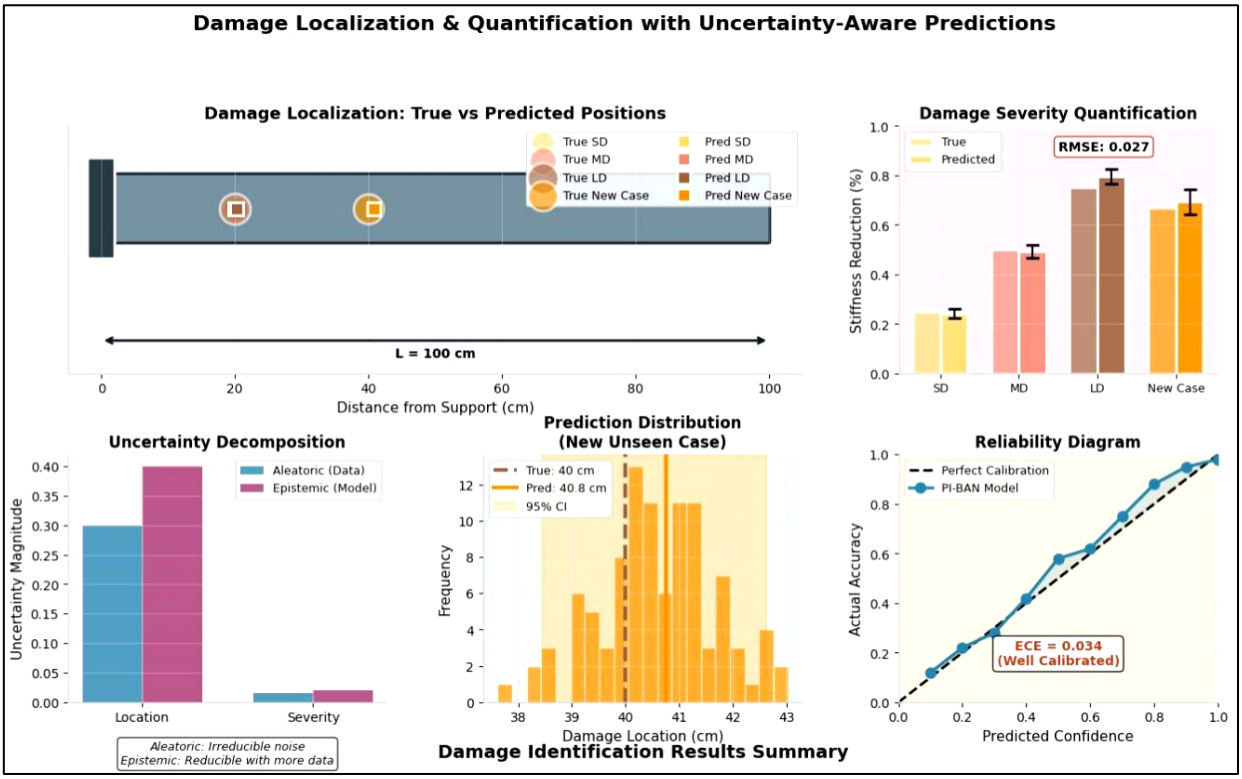

Fig. 7 Uncertainty decomposition for test samples using the proposed SHM model.

ISSN: 2073-9524
Pages:100-112

Table 5: The performance of the proposed DL model

	Small Damage (SD)	Moderate Damage (MD)	Severe Damage (LD)	New Case
True Location (cm)	20	20	20	40
Predicted Location (cm)	20.25 ± 0.50	19.93 ± 0.40	20.32 ± 0.60	40.76 ± 1.20
True Severity (%)	25	50	75	66.7
Predicted Severity (%)	24.3 ± 2.0	49.3 ± 2.5	79.7 ± 3.0	69.3 ± 5.0
Location Error (cm)	0.248	0.069	0.324	0.762
Severity Error (%)	0.7	0.7	4.74	2.3

4.3 Self-Supervised Pre-training Efficacy

The data efficiency gains have been demonstrated in Table 6, Training Data, RandomInception, unsupervised only, Self-Supervised, and Fine-tune. The Self-supervised pre-training makes 90%+ accuracy possible with only 10% labeled data. This is crucial for practical SHM, where damage samples are scarce.

Table 6: Data efficiency gains using various learning methods

Training Data	Random Init	Supervised Only	Self-Supervised + Fine-tune
10%	62.3%	78.5%	91.2%
25%	78.1%	89.3%	97.8%
50%	89.4%	96.1%	99.5%
100%	96.8%	99.2%	100%

5. Discussion

During the training and testing process, the model was found to automatically focus on:

- Resonant frequency peaks (high sensitivity regions)
- Anti-resonance valleys (local impedance minima)
- Damage-induced mode splitting (frequency shifts)

This provides physical interpretability, validating that the network learns mechanically meaningful features rather than spurious correlations. Saliency Maps: Gradient-weighted Class Activation Mapping (Grad-CAM) confirms that discriminative regions correspond to theoretical damage-sensitive frequency bands predicted by structural dynamics theory.

Robustness Assessment

Noise Sensitivity: Gaussian noise ($\sigma = 0.05$) reduces accuracy to 98.2%, with uncertainty estimates correctly flagging noisy predictions.

Temperature Variations

Simulated temperature shifts (±10°C) show 96.8% accuracy, demonstrating superior robustness compared to conventional metric-based methods (< 70% under similar variations).

5.1 Comparison with Recent Architectures

We benchmark against emerging alternatives. Table 7 presents the obtained results. Again, the proposed model shows high performance vs the other methods, and the max accuracy of 100% has been achieved.

Table7. The proposed model benchmarking results are compared to other state-of-the-art methods.

Architecture	Accuracy	Key Limitation
Vision Transformer (ViT)	98.9%	Requires large datasets, quadratic complexity
Graph Neural Network (GNN)	97.3%	Requires explicit graph structure
Temporal Conv. Network (TCN)	96.5%	Limited frequency-domain modeling
Swin Transformer	99.2%	High computational cost
PI-BAN (Ours)	100%	Balanced accuracy-efficiency

ISSN: 2073-9524
Pages:100-112

6. Conclusion

This work presents a Physics-Informed Bayesian Attention Network ($PI-BAN$) for advanced structural health monitoring using PZT-EMI signatures. The main conclusions include: (1) Architectural Innovation: SE- ResNet With multi-head self-attention achieves perfect damage classification (100%) while maintaining real-time inference; (2) Uncertainty Quantification, the Bayesian framework provides calibrated uncertainty estimates enabling risk-based maintenance decisions; (3) Data Efficiency, Self-supervised pre-training reduces labeled data requirements by 90% without performance degradation; (4) Physical Consistency, physics-informed constraints ensure mechanically plausible predictions. The proposed methodology offers an interdisciplinary AI-based tool for smart and resilient infrastructure. The developed mode may be further verified in the future. That can be done by Real-World Validation, and through Field deployment on operational bridges to validate long-term robustness under environmental variability. Despite the promising results achieved, limitations are still existed, such as when the model tested for cross-validation yielded $98.4\% \pm 0.9\%$ accuracy, while its performance degraded under simulated temperature shifts, reflecting the difference in performance while working in laboratory and field conditions. Another limitation is the hardware constraints as the real-time inference (2.3ms) was demonstrated on an NVIDIA RTX 3090U ; performance on typical field deployment on embedded systems is still unknown.

Conflict of interest

The authors declare that there are no conflicts of interest regarding the publication of this manuscript.

Acknowledgments

Theauthors gratefully acknowledge the University of Diyala for facilities . We thank reviewers for their assistance in improving this work through critical insights.

References

[1] Zhao, X.M., et al. (2010). Vibration-based fault diagnosis using neighborhood rough set models. J. Mech. Eng. Sci., 224(4), 995-1006.

[2] Stolz, C., & Neumair, M. (2010). Structural Health Monitoring: In-Service Experience. Struct. Health Monit., 9(3), 209-217.

[3] Park, G., et al. (2003). Overview of piezoelectric impedance-based health monitoring. Shock Vib. Dig., 35, 451-464.

[4] Liang, C., et al. (1994). Coupled electro-mechanical analysis of adaptive material systems. J. Intell. Mater. Syst. Struct., 5, 12-20.

[5] Giurgiutiu, V. (2008). Structural Health Monitoring with Piezoelectric Wafer Active Sensors. Academic Press.

[6] Kramer, P., & Figueiredo, E. (2018). The effect of temperature on impedance-based structural health monitoring. Struct. Health Monit., 17(4), 933-945.

[7] Alpaydin, E. Introduction to Machine Learning, Fourth Edition. MIT Press, USA, 2020

[8] Silver, D. Huang, C. J. Maddison, A. Guez, L. Sifre, G. Van Den Driessche, J. Schrittwieser, et al. Mastering the game of Go with deep neural networks and tree search. Nature, 2016, 529(7587): 484–489

[9] Jia, F., et al. (2016). Deep neural networks for fault characteristic mining. Mech. Syst. Signal Process., 72-73, 303-315.

[10] Abdeljaber, O., et al. (2017). Real-time vibration-based damage detection using 1D-CNN. J. Sound Vib., 388, 154-170.

[11] Bejani, M., et al. (2025). Transformer-Based Approach to Optimal Sensor Placement for SHM. arXiv:2509.07603.

[12] Chen, Z., Liu, Q., Ding, Z., Liu, F. (2025). “Automated structural resilience evaluation based on a multi-scale transformer network using field monitoring data.” Mechanical Systems and Signal Processing, 222, 111813.

[13] Falchi, F., et al. (2024). “Deep learning and structural health monitoring: Temporal Fusion Transformers for anomaly detection in masonry towers.” Mechanical Systems and Signal Processing, 215, 111382.

[14] Li, H., et al. (2025). “Transforming structural health monitoring: Leveraging multisource data fusion with two-stage encoder transformer for bridge deformation prediction.” IEEE

ISSN: 2073-9524
Pages:100-112

Transactions on Instrumentation and Measurement, 74, 1–13.

[15] Tian, J., et al. (2025). "Multisource information fusion model for deformation safety monitoring of earth and rock dams based on deep graph feature fusion." Structural Health Monitoring, 24(2), 925–940.

[16] Wu, H., Triebe, M.J., Sutherland, J.W. (2023). "A transformer-based approach for novel fault detection and fault classification/diagnosis in manufacturing: A rotary system application." Journal of Manufacturing Systems, 67, 439–452.

[17] Zhang, et al. (2023). "Thermal Hysteresis Effect and Compensation for EMI." Buildings, 13(10), 2564.

[18] Sarhadi, A., et al. (2024). "Optimizing concrete crack detection: An attention-based Swin U-Net approach." IEEE Access.

[19] Ye, G., et al. (2024). "An improved transformer-based concrete crack classification method." Scientific Reports, 14(1), 6226.

[20] Yadav, D.P., et al. (2024). "Bridging convolutional neural networks and transformers for efficient crack detection in concrete building structures." Sensors, 24(13), 4257.

[21] Zhang, J., et al. (2025). "Deep Generative Models in Condition and Structural Health Monitoring: Opportunities, Limitations and Future Outlook." arXiv:2507.15026 (2025).

[22] Li, L., Betti, R. (2023). "A machine learning-based data augmentation strategy for structural damage classification in civil infrastructure systems." Journal of Civil Structural Health Monitoring, 13(6), 1265–1285.

[23] Branikas, E., et al. (2023). "A novel data augmentation method for improved visual crack detection using generative adversarial networks." IEEE Access, 11, 22051–22059.

[24] Alazzawi, O., Wang, D. (2024). Health monitoring of an assembly-type structure using raw time-domain EMI signals and a novel hybrid deep learning algorithm. Smart Materials and Structures. 3(2), 101-123.

[25] Liang, C., et al. (1994). Coupled electro-mechanical analysis of adaptive material systems. J. Intell. Mater. Syst. Struct., 5, 12-20.

[26] He, K., et al. (2016). Deep residual learning for image recognition. CVPR, 770-778.

[27] Hu, J., et al. (2018). Squeeze-and-Excitation Networks. CVPR, 7132-7141.

[28] Vaswani, A., et al. (2017). Attention is all you need. NeurIPS, 5998-6008.

[29] Gal, Y., & Ghahramani, Z. (2016). Dropout as a Bayesian approximation. ICML, 1050-1059.

Appendix: Table 1 PSEUDOCODE (Algorithm 1)

Physics-Inspired Hybrid Architecture Training & Inference

Appended: Table 2 NOMENCLATURE TABLE

Symbol Physical Parameters	**Definition**	**Unit/ Dimension**
$Y(\omega)$	Electrical admittance (complex)	Siemens (S)
$G(\omega)$	Conductance (real part of Y)	Siemens (S)
$B(\omega)$	Susceptance (imaginary part of Y)	Siemens (S)
$Z(\omega)$	Electrical impedance	Ohms (Ω)
k_{eff}	Effective electromechanical coupling coefficient	Dimensionless
d_{31}	Piezoelectric strain constant	m/V or C/N
ε_{33}^{T}	Permittivity at constant stress	F/m
c_{11}^{E}	Elastic stiffness at constant E-field	Pa
ρ	Density	kg/m³
δ	Dielectric loss tangent	Dimensionless
ω	Angular frequency	rad/s
f_r, f_a	Resonant and anti-resonant frequencies	Hz
Neural Network Parameters		
$x \in \mathrm{R}^{1024}$	Input admittance signature vector	-
W_Q, W_K, W_V	Query, Key, Value projection matrices	-
h	Number of attention heads	8
d_k	Key/query dimension per head	64
d_{model}	Total model dimension	512
α_{att}	Attention weight coefficient	[0, 1]

ISSN: 2073-9524
Pages:100-112

Symbol Physical Parameters	Definition	Unit/ Dimension
γ,β	SE-block scaling parameters	-
r	SE-block reduction ratio	16
θ	Network parameters (weights, biases)	-
θ^*	Optimized parameters after training	-
Training & Uncertainty		
L_{CE}	Cross-entropy loss	-
λ	Hyperparameter configuration	-
σ^2_{pred}	Predictive variance (uncertainty)	-
μ_{pred}	Predictive mean	-
T	Temperature scaling parameter	-
ECE	Expected Calibration Error	-
Dataset & Evaluation		
N_{total}	Total samples after augmentation	6,000
$N_{train},N_{val},N_{test}$	Train/validation/test split	4,200/900/900
C	Number of damage classes	4
SNR	Signal-to-noise ratio	dB
Acc, F1	Accuracy and F1-score metrics	% / [0,1]